

ANALYSIS OF THE SST SPLIT-WINDOW EQUATION USING THE SYNERGY BETWEEN METEOSAT SECOND GENERATION AND NOAA POLAR SATELLITES

José Antonio Valiente, Raquel Niclòs, María Jesús Barberá and María José Estrela

Fundación CEAM, C/ Charles R Darwin 14, 46980 Paterna, Valencia, Spain.

Abstract

In its first stage, the study uses AVHRR NOAA/NESDIS SST and SEVIRI O&SI SAF SST operational algorithms to compare SST values derived from concurrent AVHRR and MSG scenes centred on the Iberian Peninsula and western Mediterranean sea. The comparison is performed on a set of paired AVHRR and SEVIRI images spaced no more than 10 minutes apart, and obtained from the high resolution transmissions from both MSG1 and NOAA-12, -15 and -17 series during the year 2005. The SST agreement is good for small AVHRR zenith angles but discrepancies are observed for angles larger than 40° . In the second stage of the study, a general split-window equation combining two addends, one for the atmospheric correction and the other for an emissivity effect, is proposed to account for the observed differences in SST at large AVHRR angles. The functional form of the proposed equation is the same for both satellites, and its angular dependence is considered to be implicit in the emissivity term. As the split-window channel filters are almost identical for both AVHRR and SEVIRI, concurrent spatial and temporal pairs of satellite data with almost identical zenith angles are regressed to the atmospheric correction term of the proposed equation. This enables resolving the atmospheric split-window coefficients and subsequently estimating the emissivity term. We then carry out a simple variable substitution when one of the paired satellite zenith angles cancels and a successive value propagation when the paired zenith angles differ, to finally yield a plotting of the dependence of the emissivity term on the satellite zenith angle.

INTRODUCTION

Most of the operational algorithms for estimating Sea Surface Temperature (SST) are derived by means of multi-linear regression to a family of proposed equations that combine brightness temperatures (BT) in different channels (Barton, 1995). Multi-channel algorithms, MCSST, are obtained in this way by combining coefficients that can be either constants (McClain *et al.*, 1985) or expressed in terms of $\sec(\theta)-1$ where θ is the satellite zenith angle (François *et al.*, 2002). Additionally, when the proposed equations include a first-guess SST in one of the coefficients, the algorithm is denominated nonlinear or NLSST (Walton *et al.*, 1998). The NLSST algorithms are routinely selected by NOAA and EUMETSAT for an operational use.

The data used for the multi-linear regression are obtained either empirically or by means of simulations. The empirical procedure uses satellite derived SST data paired with concurrent temperature measurements from buoys for a period of time, the so-called SST match-up datasets (Li *et al.*, 2001). In the simulation procedure, a radiative transfer model is used for calculating synthetic radiances received by the satellite under specific conditions: a set of actual radiosoundings determining the atmospheric profiles, the satellite zenith angles, sea surface temperature and sea surface emissivity (François *et al.*, 2002).

None of the operational family of equations uses a residual term to account for the emissivity of the sea surface. Conversely, operational split-window algorithms for Land Surface Temperature (LST) retrieval include emissivity-dependent terms (Becker & Li, 1990; Coll & Caselles, 1997; Wan *et al.*,

2002). The emissivity of the sea surface is very different from a blackbody at moderate to large observation angles. It decreases as the angle increases, and it also varies as surface roughness changes (Masuda *et al.*, 1988; Wu & Smith, 1997; Niclòs *et al.*, 2005). Some operational algorithms include sea-surface emissivity implicitly when performing the regression, some consider emissivity close to unity, and some are limited to a narrow range of observation angles where surface emissivity is practically constant. Therefore, the emissivity effect is to be examined explicitly and within its whole angular range on the SST retrieval mainly at medium to large observation angles.

SATELLITE DATA AND OPERATIONAL SST COMPARISON

During the year 2005, a set of concurrent images spaced no more than 10 minutes apart in time was selected from the high resolution transmissions from both MSG1 and NOAA-12, -15 and -17 series. One complete day for each month was captured from the transmissions, normally providing six concurrent satellite scenes for any 24-hour period chosen. The selection of each of the specific days was based mainly on cloud clearing over the oceanic surfaces. This gave a good cover over the Mediterranean Sea but few scenes over the Atlantic Ocean due to frequent cloudy conditions. Cloudy pixel removal was performed on AVHRR and SEVIRI scenes using the cloud filters proposed by Derrien *et al.* (1993) and Derrien & Le Gléau (2005) for both nocturnal and diurnal conditions over the sea. Conversion to brightness temperatures followed Goodrum *et al.* (2000) and Tjemkes (2005).

Both SEVIRI and AVHRR scenes are referenced to the same geographical framework, a stereographic projection centred at the Iberian Peninsula, for pixel spatial conformity (Badenas *et al.*, 1997; Wolf & Just, 1999; Dammann *et al.*, 2005). AVHRR and SEVIRI satellite-derived SST were estimated using the non-linear operational algorithms (NLSST) supplied from NOAA/NESDIS CoastWatch equations (DiGiacomo, 2005) and Meteo-France O&SI SAF equations (OSI SAF Project Team, 2005), respectively. These operational temperatures are used for the sole purpose of evaluating the two algorithm performances at a range of zenith angles and temperatures.

As an example of the SST comparison for a particular pair of AVHRR and SEVIRI scenes, figure 1 shows operational SST differences on June 19th 2005 at 17:45 GMT (MSG) and 17:55 GMT (NOAA-15). Blank areas correspond to either removed clouds or absence of AVHRR data. While SEVIRI zenith angles move in the range of 40° to 60°, AVHRR angles show values from 0° to almost 70°. Solid lines show identical zenith angles for the pair of scenes. Broken lines identify AVHRR zenith angles of 40° and 60°. One can observe that satellite SST differences are under -1 °C when AVHRR angles are larger than 60°. For evaluating the goodness of a comparison of both SST operational algorithms, AVHRR zenith angles should be limited to a maximum of 40° as figure 1 shows, so that the associated algorithm uncertainties, about 0.5 °C, are comparable to the obtained SST differences.

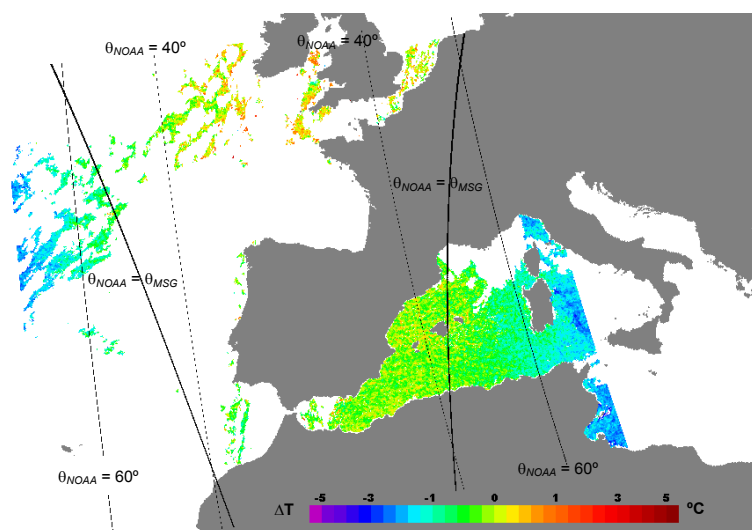


Figure 1: Operational SST differences for a particular pair of simultaneous AVHRR and SEVIRI scenes.

For the comparison of NOAA/NESDIS and Meteo-France OSI SAF operational NLSST algorithms, a cluster of points (figure 2) was selected from the image set. Since a good comportment of the comparison points was sought, the following conditions were observed in their selection: absence of cloudiness in each pair of satellite scenes, AVHRR satellite zenith angles below 30° , random spatial distribution but regular spacing within the range of 10-28 °C for SST, and a limited maximum total number. The SST comparison performed for the cluster of selected points is given in figure 3. The diagonal line represents the 1:1 relation, with the standard deviation around this line being about 0.4 °C. As a first result, the SST correspondence between both algorithms when restrictions in the AVHRR zenith angle are considered is comparable to the estimation errors which are intrinsically associated with each of the non-linear algorithms.

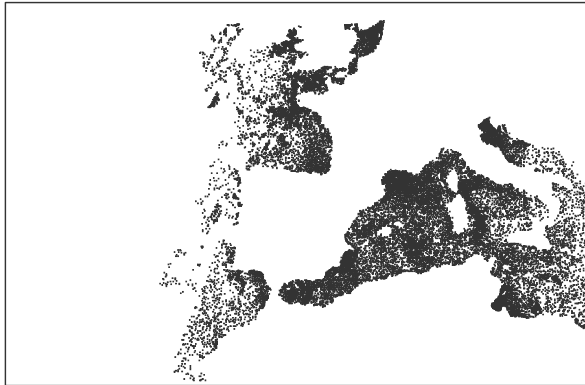


Figure 2: Selection of 30,000 points from the synergy between AVHRR and SEVIRI, used for the comparison of operational NLSST algorithms

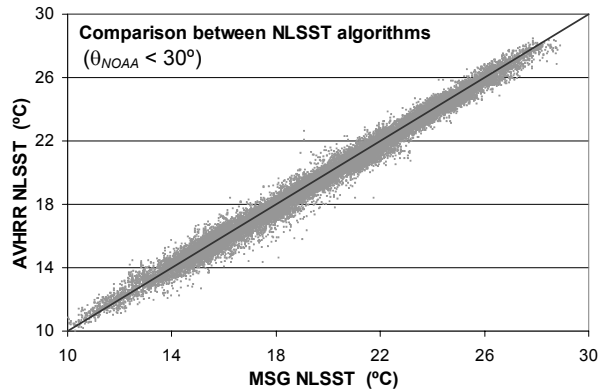


Figure 3: Comparison of SSTs derived from the two operational algorithms when the selection of points is used, i.e. AVHRR zenith angles are low.

If no restrictions in AVHRR zenith angles are considered, the comparison obtained for the NOAA/NESDIS and OSI SAF algorithms is given in figure 4. This comparison uses a more spread-out cluster of points than the one represented in figure 2, accounting in this manner for large satellite zenith angles occurring in the AVHRR scenes. The difference between AVHRR-derived and SEVIRI-derived temperatures shows a decline as the AVHRR zenith angle increases in the form of $S = \sec(\theta) - 1$. The zenith angle must be stretched in this form to display the rapid decline. At low AVHRR zenith angles, below $\theta = 40^\circ$ or $S = 0.3$, both algorithms coincide. For AVHRR angles as large as $\theta = 69^\circ$ ($S = 1.8$), the differences between AVHRR-derived and SEVIRI-derived operational SSTs can be around -2 °C.

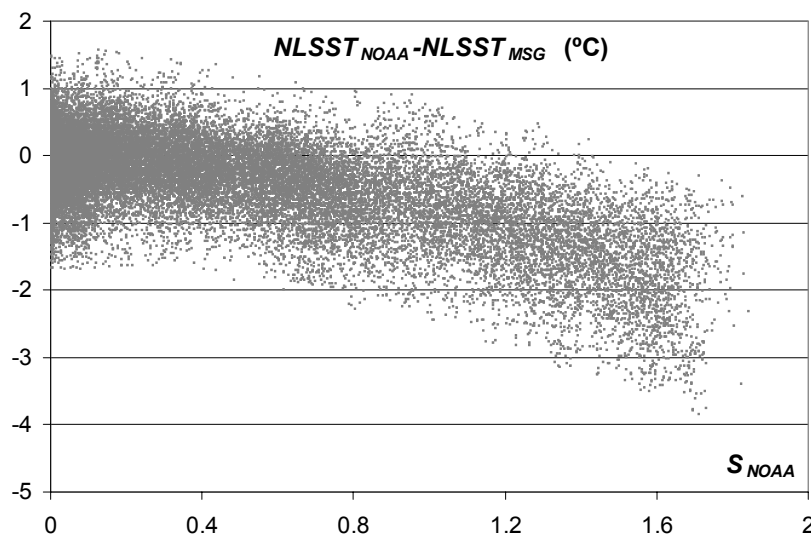


Figure 4: Difference values between AVHRR-derived and SEVIRI-derived temperatures using the operational NLSST algorithms from NOAA/NESDIS and Meteo-France OSI/SAF when no AVHRR zenith angle limit is considered. Values are plotted against AVHRR zenith angle in its S form, $S = \sec(\theta) - 1$.

The fact that the derived SST differences behave as a function of the AVHRR zenith angle could be explained by the effect of the significant angular dependence of sea surface emissivity. It is already known that for large zenith angles, emissivity shows a strong decline, and it is also dependent on the sea surface roughness produced by wind (Wu & Smith, 1997). The angular range where the NOAA/NESDIS NLSST algorithm has been tested is much larger than the angular range for the OSI SAF NLSST algorithm, i.e. the typical range around the Iberian Peninsula. Then, the angular dependence of the SST differences found is very evident in the case of the AVHRR zenith angle. It can be expected also that some emissivity effect is also influencing the SEVIRI-derived temperatures to the extent of its angular range. If this angular dependence of the surface emissivity is not correctly considered in the SST algorithms, differences in derived temperatures, such as the observed in figure 4, could be obtained for large satellite zenith angles. In the next section, we propose a split-window equation with a single functional form, which includes an emissivity term and can be used with both SEVIRI and AVHRR scenes. Using only the empirical satellite brightness temperatures, we have devised a method to obtain angle information on the above-mentioned emissivity effect.

REGRESSION OF A SPLIT-WINDOW EQUATION WITH NO ANGLE LIMIT

Including a sea surface emissivity effect in the SST split-window equation is essential when emissivity variability exists. The following generic split-window equation based on Coll & Caselles (1997) includes both an atmospheric correction expressed as a function of brightness temperatures and a residual term dependent on emissivity:

$$SST = a_0 + a_1 T_i + a_2 T_{ij} + a_3 T_{ij}^2 + \gamma(\varepsilon)$$

where:

a_i are taken as constants for each of the satellite sensors

T_i is the brightness temperature, BT, of channel i at 11 μm (ch4 for AVHRR and ch9 for SEVIRI)

T_{ij} is the difference $T_{ij} = T_i - T_j$ with T_j being the BT of channel j at 12 μm (ch5 for AVHRR and ch10 for SEVIRI)

$\gamma(\varepsilon)$ is a residual term dependent on the sea surface emissivity, ε , which in turn will depend basically on the satellite zenith angle, θ , and to a lower degree on the atmospheric water vapour, W (Nicolòs *et al.*, 2007)

Adapting this equation for each of the AVHRR and SEVIRI sensors on board the NOAA and MSG satellites respectively, i.e. substituting the thermal channels at 11 and 12 μm with their specific channel numbers, the equation becomes:

$$SST_{NOAA} = a_0 + a_1 T_4 + a_2 T_{45} + a_3 T_{45}^2 + \gamma(\varepsilon_{NOAA})$$

$$SST_{MSG} = b_0 + b_1 T_9 + b_2 T_{910} + b_3 T_{910}^2 + \gamma(\varepsilon_{MSG})$$

The spectral filters of the thermal channels at 11 and 12 μm for MSG and NOAA satellites are practically coincident (Goodrum *et al.*, 2000), especially for NOAA-15 and -17. Thus, a surface spot seen simultaneously from the two satellites, MSG and NOAA, at equal zenith angles will yield identical residual emissivity terms, since channel emissivities will match for confluent bands.

$$\gamma(W, S_{NOAA}) = \gamma(W, S_{MSG}) \quad \text{when } S_{NOAA} = S_{MSG}$$

And as the sea surface pixel is at a unique temperature, it must follow that:

$$SST = SST_{NOAA} = SST_{MSG}$$

So, for the group of pixel pairs that meet the condition of being observed from the same zenith angle maintained by both satellites, it is possible to fit the following multi-linear form to their brightness temperatures:

$$a_0 + a_1 T_4 + a_2 T_{45} + a_3 T_{45}^2 = b_0 + b_1 T_9 + b_2 T_{910} + b_3 T_{910}^2$$

Making $c_0 = a_0 - b_0$, $\alpha_i = a_i/c_0$ and $\beta_i = b_i/c_0$, a proper expression for the multi-linear regression would be:

$$\alpha_1 T_4 + \alpha_2 T_{45} + \alpha_3 T_{45}^2 - \beta_1 T_9 - \beta_2 T_{910} - \beta_3 T_{910}^2 = -1$$

Figure 5 shows the comparison of the partial temperature terms given by the above multi-linear expression when fitted to the brightness temperatures whose zenith angle pairs fulfil the condition $\Delta S < 0.05$. This is the same as saying that the pixel pairs used for the regression practically coincide in zenith angle. Data points spread out along a defined line indicate the goodness of the regression. The numerical analysis is done hereafter for only the synergy between MSG and NOAA-17 in diurnal conditions due to the larger and better quality of their data. The other NOAA satellites provide analogous results, although their data points show a greater scattering.

Once the above regression coefficients have been obtained, the known NOAA/NESDIS operational NLSST algorithm is used for the computation of the remaining parameters c_0 and a_0 , necessary for a complete solution of the problem. This operational algorithm must be used at the particular zenith angular range where the residual term due to the emissivity effect is negligible, i.e., for zenith angles $\theta < 10^\circ$ for example. At this angle range, a contribution from any emissivity effect would be incorporated in the constants a_0 and b_0 , thus making the proposed emissivity effect become zero at very low zenith angles.

$$NLSST_{NOAA} = a_0 + a_1 T_4 + a_2 T_{45} + a_3 T_{45}^2 = a_0 + c_0 (\alpha_1 T_4 + \alpha_2 T_{45} + \alpha_3 T_{45}^2) \quad \text{for } \theta_{NOAA} < 10^\circ$$

The above equation can be fitted as a straight line to the satellite data. In this manner, figure 6 gives the resultant fitting for NOAA-17 in diurnal conditions. The values found for c_0 and a_0 allow the estimation of parameter b_0 and subsequently the determination of coefficients a_i and b_i .

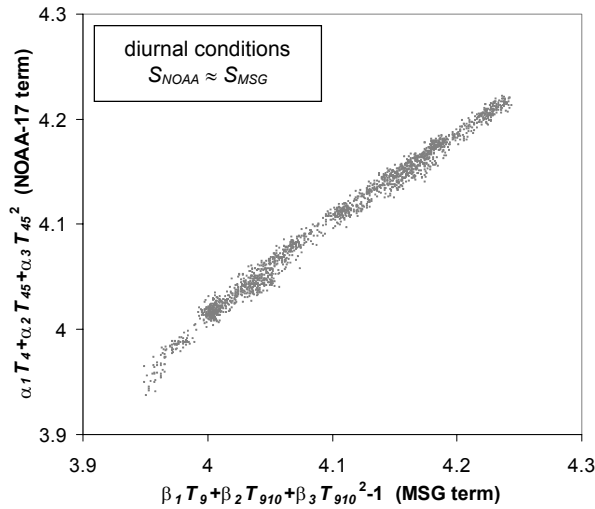


Figure 5: Goodness of the regression to the atmospheric correction term for the data pairs with practically the same zenith angles. Data correspond to NOAA-17 versus MSG in diurnal conditions.

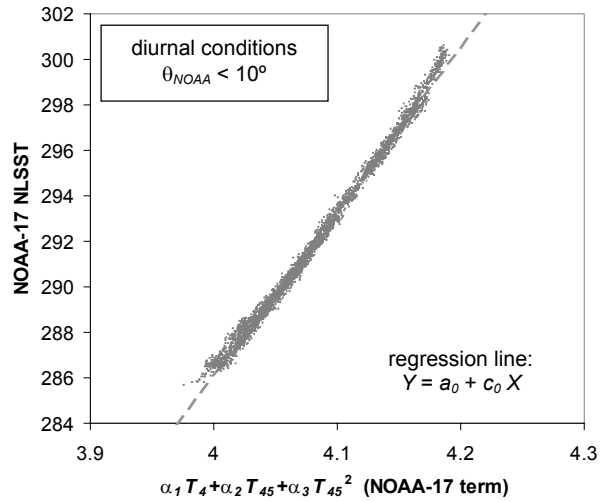


Figure 6: Straight line fitting to derive remaining parameters c_0 and a_0 in the characterisation of the proposed split-window coefficients for the atmospheric correction term. Again data correspond to NOAA-17 in diurnal conditions.

PLOTTING OF THE RESIDUAL EMISSIVITY TERM USING THE SYNERGY BETWEEN MSG AND NOAA

For each pair of simultaneous AVHRR and SEVIRI scenes, any coincident pixel must present a single and identical sea surface temperature. Moreover, each coincident pixel in both scenes is observed generally from two different zenith angles depending on the satellite used, MSG or NOAA. Therefore, the difference between the residual terms due to the emissivity effect for the coincident pixels

observed from zenith angles S_{MSG} and S_{NOAA} can be expressed, in terms of the split-window coefficients found, by the following multi-linear equation:

$$\gamma(S_{MSG}) - \gamma(S_{NOAA}) = a_0 + a_1 T_4 + a_2 T_{45} + a_3 T_{45}^2 - b_0 - b_1 T_9 - b_2 T_{910} - b_3 T_{910}^2$$

This equation assumes that the possible dependence introduced by water vapour, W , in the residual terms is minimal since its variability is low in the study region. Now, data values for the new function $\{\gamma(S_{MSG}) - \gamma(S_{NOAA})\}$ can be gathered using the set of satellite data pairs from MSG and NOAA. However, this is not the sought-after function but the residual term $\gamma(S)$ dependent on only a single angle variable S . An iterative process has been devised for turning the difference function into the sought-after residual term by means of boundary conditions. First, when $S_{NOAA} \approx 0$ for an AVHRR point, its SEVIRI pair will determine the value for $S = S_{MSG}$ where $\gamma(S)$ can be obtained, since $\gamma(S_{NOAA}) \approx 0$. Once a sufficient number of γ values against S are gathered, they can be substituted into the above expression when any of the obtained S s coincides with any of the observation angles for the AVHRR and SEVIRI pairs. This iterative process can be expressed graphically in the following steps:

$$\begin{aligned} \text{if } S_l \approx 0 & \quad \text{then } \gamma(S_k) = \{\gamma(S_k) - \gamma(S_l)\} \\ & \quad \text{and } \gamma(S_m) = \gamma(S_k) - \{\gamma(S_k) - \gamma(S_m)\} \\ & \quad \text{and so on ...} \end{aligned}$$

Figure 7 shows the scatter plot resulting from the iterative process to yield the residual term γ against the angle parameter S . Data were obtained from the synergy between MSG and NOAA-17 in diurnal conditions. Similar results were also obtained using the synergy between MSG and the other NOAA satellites and solar conditions, although a larger level of scattering was observed. Values for the residual term γ are scattered in the plot following a clear ascending tendency as the zenith angle increases according to parameter S . As a first approximation, a quadratic curve can be fitted to the scattering of points yielding the expression that is provided in the figure. The fitting does not consider any data weighting based on scattering density and it is constrained to be zero at nadir.

In addition to the ascending tendency of the emissivity term with zenith angle, a large scattering is also visible in the figure. The scattering is around 2 to 3 °C wide in most of the angular range, and about 4 °C at the origin. The scattering is difficult to explain and could be due to different sources: error propagation of the multi-linear regression technique dependent on data collection, errors associated with the estimation of brightness temperatures which are not very accurate in the case of MSG1, and dependence of the residual term on factors other than the satellite zenith angle alone.

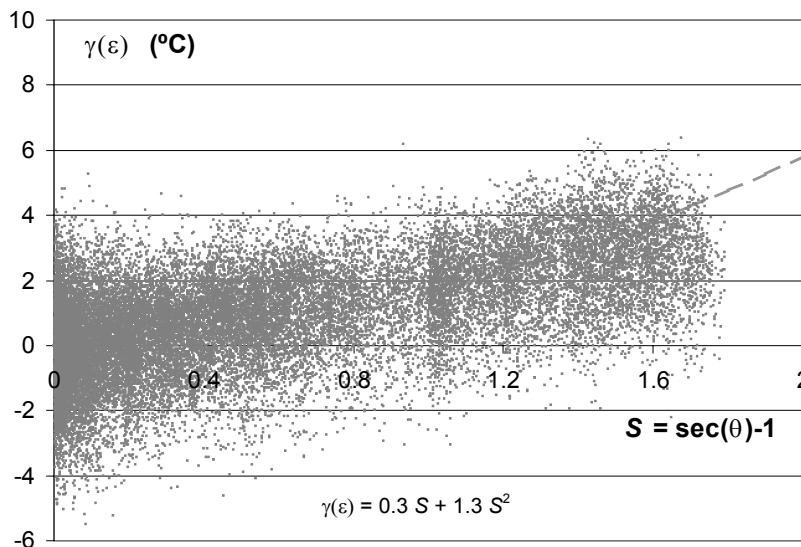


Figure 7: Obtained values for the residual term γ of the emissivity effect as a function of the angle parameter S . Data correspond to the synergy between MSG and NOAA-17 satellites in diurnal conditions. The quadratic curve represents the ascending tendency that is gathered from the data scattering.

CONCLUSIONS

The study has shown how operational NLSST algorithms can work incompletely for large observation angles. This can be due to the lack of an emissivity term which is normally considered only in models that have been developed on physical basis. Then, zenith angle limitations should be expected in operational algorithms that are obtained without considering the specific surface emissivity angular variability. Besides, using only AVHRR and SEVIRI satellite data, it is possible to reveal the behaviour of a residual term which is dependent on surface emissivity and takes part in the split-window equation of a physical model. This result supports the functional form of a SST split-window equation into two terms: one for the atmospheric correction and the other for the sea surface emissivity effect.

Recently, Nicolòs et al. (2007) have provided a split-window equation that incorporates an emissivity term obeying a physical model. They use atmospheric profiles and both sea surface and atmospheric radiative models to derive a collection of simulated temperatures for which the coefficients of a quadratic split-window equation are estimated. The functional form of their residual emissivity term has shown similar behaviour to the one presented here. Differences involve more scattering and a slightly larger increasing tendency found in our study. The present work uses satellite data as the only source of experimental data, so the obtained algorithm coefficients may depend strongly on the range covered. Besides, precision errors associated with the conversion of MSG data to satellite radiances (Eumetsat, 2007) are a matter of concern in explaining the observed scattering. The influence of water vapour content and surface wind on the residual emissivity term also needs to be considered.

ACKNOWLEDGEMENTS

This research was supported by the Spanish Ministry of Education and Science, project number REN2003-09771, and a "Juan de la Cierva" Research Contract for Dr Nicolòs. Access to Meteosat Data has been obtained from EUMETSAT through a license agreement for research project, EUM/MSG/03/990040294. The manuscript was revised by J. Scheiding. Fundación CEAM is supported by the Generalitat Valenciana and BANCAIXA.

REFERENCES

- Badenas, C, Caselles, V, Estrela, MJ, Marchuet, R, (1997) Some improvements on the process to obtain accurate maps of sea surface temperature from AVHRR raw data transmitted in real time. Part 1: HRPT images. *International Journal of Remote Sensing*, **18**, pp 1743-1767
- Barton, IJ, (1995) Satellite-derived sea surface temperatures: Current status. *Journal of Geophysical Research*, **100**, pp 8777-8790
- Becker, F, Li, ZL, (1990) Towards a local split-window method over land surfaces. *International Journal of Remote Sensing*, **11**, pp 369-394
- Coll, C, Caselles, V, (1997) A split-window algorithm for land surface temperature from advanced very high resolution radiometer data: Validation and algorithm comparison. *Journal of Geophysical Research*, **102**, pp 16697-16714
- Dammann, K, Mueller, J, Hanson, C, Gärtner, V, Flewin, J, Williams, M, (2005) MSG Level 1.5 image data format description. EUMETSAT, issue 3, EUM/MSG/ICD/105, 208 p
- Derrien, M, Farki, B, Harang, L, Le Gléau, H, Noyalet, A, Pochic, D, Sairouni, A, (1993) Automatic cloud detection applied to NOAA-11 / AVHRR imagery. *Remote Sensing of Environment*, **46**, pp 246-267
- Derrien, M, Le Gléau, H, (2005) MSG/SEVIRI cloud mask and type from SAFNWC. *International Journal of Remote Sensing*, **26**, pp 4707-4732
- DiGiacomo, P, (2005) CoastWatch Program. NOAA's National Environmental Satellite Data and Information Service (http://oceanwatch.noaa.gov/ow_index.html)

- Eumetsat (2007) A planned change to the MSG Level 1.5 image product radiance definition. Document number EUM/OPS-MSG/TEN/06/0519, issue v1A, Darmstadt, 9 p
- François, C, Brisson, A, Le Borgne, P, Marsouin, A, (2002) Definition of a radiosounding database for sea surface brightness temperature simulations. Application to sea surface temperature retrieval algorithm determination. *Remote Sensing of Environment*, **81**, pp 309-326
- Goodrum, G, Kidwell, KB, Winston, W, (2000) NOAA KLM user's guide and recent amendments. U.S. Department of Commerce, National Oceanic and Atmospheric Administration, National Environmental Satellite, Data, and Information Service (<http://www2.ncdc.noaa.gov/docs/klm/cover.htm>)
- Li, X., Pichel, WG, Maturi, E, Clemente-Colón, P, Sapper, J, (2001) Deriving the operational nonlinear multichannel sea surface temperature algorithm coefficients for NOAA-15 AVHRR/3. *International Journal of Remote Sensing*, **22**, pp 699-704
- Masuda, K, Takashima, T, Takayama, Y, (1988) Emissivity of pure and sea waters for the model sea surface in the infrared window regions. *Remote Sensing of Environment*, **48**, pp 302-308
- Mcclain, EP, Pichel, WG, Walton, CC, (1985) Comparative performance of AVHRR-based multichannel sea-surface temperatures. *Journal of Geophysical Research*, **90**, pp 11587-11601
- Niclòs, R, Valor, E, Caselles, V, Coll, C, Sanchez, JM, (2005) In situ angular measurements of thermal infrared sea surface emissivity - validation of models. *Remote Sensing of Environment*, **94**, pp 83-93
- Niclòs, R, Caselles, V, Coll, C, Valor, E, (2007) Determination of sea surface temperature at large observation angles using an angular and emissivity-dependent split-window equation. *Remote Sensing of Environment*, **111**, pp 107-121
- OSI SAF Project Team, (2005) Atlantic sea surface temperature product manual. Ocean & Sea Ice Satellite Application Facility, Meteo-France, version 1.5, SAF/OSI/M-F/TEC/MA/121, 43 p
- Tjemkes, SA, (2005) On the Conversion from Radiances to Equivalent Brightness Temperatures. EUMETSAT, 24 p
- Walton, CC, Pichel, WG, Sapper, JF, May, DA, (1998) The development and operational application of nonlinear algorithms for the measurement of sea surface temperatures with the NOAA polar-orbiting environmental satellites. *Journal of Geophysical Research*, **103**, pp 27999-28012
- Wan, Z, Zhang, Y, Zhang, Q, Li, Z, (2002) Validation of the land-surface temperature products retrieved from terra moderate resolution imaging spectroradiometer data. *Remote Sensing of Environment*, **83**, pp 163-180
- Wolf, R, Just, D, (1999) LRIT/HRIT global specification. Coordination Group for Meteorological Satellites, issue 2.6, CGMS 03, 53 p
- Wu, X, Smith, WL, (1997) Emissivity of rough sea surface for 8-13 m: Modelling and verification. *Applied Optics*, **36**, pp 2609-2619